Natural Hazards
and Earth System
Sciences
Discussions

Morphological analysis of hummocks in debris avalanche deposits around Mt Erciyes, central Turkey

Yuichi S. Hayakawa[1], Hidetsugu Yoshida[2], Hiroyuki Obanawa[3], Ryutaro Naruhashi[4], Koji Okumura[5], Masumi Zaiki[6], Ryoichi Kontani[7]

5 [1]Center for Spatial Information Science, The University of Tokyo, Kashiwa, 277-8568, Japan
[2]School of Arts and Letters, Meiji University, Tokyo, 101-8301, Japan
[3]VisionTech Inc., Tsukuba, 305-0045, Japan
[4]Earthquake Research Institute, The University of Tokyo, Tokyo, 113-0032, Japan
[5]Department of Geography, Graduate School of Letters, Hiroshima University, Hiroshima, 739-852, Japan
10 [6]Department of Economics and Business, Faculty of Economics, Seikei University, Tokyo, 180-8633, Japan
[7]Department of Contemporary Sociological Studies, Faculty of Literature, Notre Dame Seishin University, Okayama, 700-8516, Japan

Correspondence to: Yuichi S. Hayakawa (hayakawa@csis.u-tokyo.ac.jp)

15 **Abstract.** Debris avalanche caused by the sector collapse of a volcanic mountain often forms characteristic depositional landforms including hummocks. Not only sedimentological but also geomorphological analyses of debris avalanche deposits (DAD) are crucial to clarify the size, mechanisms, and processes of the debris avalanche. We investigate the morphology of hummocks newly identified in the DAD at the north-eastern flank of Mt. Erciyes in Kayseri, central Turkey, likely formed in the late Pleistocene. Using a remotely piloted aircraft system (RPAS) and the structure-from-motion multi-view stereo photogrammetry (SfM), we obtained high-definition digital elevation model (DEM) and orthorectified image of the DAD surface with hummocks. Detailed geometric features of the hummocks are investigated using the RPAS-derived high-definition DEM. The source volume of the DAD was also estimated by reconstructing the original shape of the mountain body using a lower-resolution satellite-based DEM. For this, topographic cross sections are examined based on the slopes around the scar that are regarded as the remnant topography preserved since the sector collapse. The spatial distribution of hummocks shows an unusual pattern regarding the distance-size relationships, i.e., anomalously concentrated in a certain distance from the source. The hummocks are found to be aligned toward the flow direction of the debris avalanche, suggesting the extensional regime of the debris avalanche. These facts indicate that this debris avalanche did not follow the typical flow type of debris avalanches observed in the other cases. Instead, the topographic constraints by former caldera wall and fault-induced lineaments could have strongly affected the flow course and pattern in this particular case: The pre-existing caldera wall topography could have acted as the topographic barriers for the debris avalanche to force the initial flow to turn northward, and the flow regime to be once compressional followed by extensional at the narrow and steepened outlet valley. Also, the estimated volume of the DAD 12–15 × 10^8 m^3 gives its mean thickness of 60–75 m, which is much deeper than the reported cases of other DADs. This suggests that the debris avalanche could have flown down to the far downstream areas from the presently-observed limit of the DAD extent. Assessments of the DAD including the results of this study can provide further insights into the risk and mitigation of potential disasters in the study area.

1 Introduction

Catastrophic sector collapses have often been observed in volcanoes when they become structurally and gravitationally unstable, and are triggered by earthquakes, the intrusion of magma, or phreatic eruptions (Siebert, 1984, 1992; Ui et al., 2000). This phenomenon is highly hazardous because of a large amount of mass movement, which appears as a debris 40 avalanche moving at high speed to widespread areas (Ui, 1975; Vallance et al., 1995; Glicken, 1996; Vallance and Scott,

1997; Yoshida and Sugai, 2006). Furthermore, sector collapse can repeatedly occur at the same volcano, which rapidly grows to form its unstable mountain body (Tibaldi and Vezzoli, 2004; Zernack et al., 2009).

Debris avalanche caused by the sector collapse of a volcanic mountain often forms characteristic depositional landforms including hummocks, which are composed of large block facies among matrix, originated from the pre-existed
5   mountain body (Siebert, 1984; Ui et al., 1986, 2000; Orton, 1996). Within the domain of debris avalanche deposits (DAD), hummocks often have clear boundaries and are readily identifiable, thus providing a chance to carry out the robust size and shape analysis (Mizuno, 1958; Hashimoto et al., 1979). Such the morphology of hummocks, located on the surface of DADs, can be used to estimate the characteristics of the debris avalanche, i.e., the kinematics of the sliding mass of the sector collapse (Dufresne and Davies, 2009; Koarai et al., 2008; Yoshida and Sugai, 2010; Yoshida, 2012, 2013, 2014; Yoshida et
10   al., 2012). Although sedimentological investigations of the internal structures of DADs often provide insights into the transport mechanisms (e.g., Glicken, 1996; Bernard et al., 2008; Shea et al., 2008), geomorphological or geometrical analyses of the surficial morphology of DADs including hummocks can also provide estimations on the size and processes of the debris avalanche. In particular, because the sedimentary structure is mutually related to the hummock distribution and shape, the distribution and morphology of hummocks formed in DADs provide an opportunity to examine the volumetric
15   and kinematic characteristics of the debris avalanche (Dufrense and Davies, 2009; Yoshida and Sugai, 2010; Yoshida et al., 2012). During the sliding of a sector collapse, the fractured mass of the original volcanic edifice forms collapse structures along with the alternate regimes of extension and compression (Paguican et al., 2012, 2014). This often results in the alternate extensional/compressional structures of DADs along the avalanche course, while the compressional regime may result in the denser distribution of hummocks particularly around the front of DADs (Yoshida et al., 2012).

20   Because the typical size of hummocks is on the order of tens to hundreds of meters, stereo-paired aerial photographs have often been used for the detection and morphological analysis of hummocks (Glicken, 1996; Yoshida, 2012, 2013, 2014; Yoshida and Sugai, 2010; Yoshida et al., 2012). High-resolution topographic data by airborne laser scanning (ALS), i.e., 1–5 m resolution digital elevation models (DEM), can also be used for such analysis (e.g., Hayakawa et al., in press). However, such high-resolution data including paired aerial photographs and ALS-DEMs are often unavailable in many areas. High-
25   resolution satellite remote sensing imagery and DEMs derived from such satellite imagery is another possible source for the analysis of hummocks, but the cost of acquisition of the data is often high and may not be readily obtained in many cases. Due to the limitation of the availability of high-resolution aerial or satellite image data and DEMs, details of many DADs remain unexamined even if the presence of such DADs is known.

Recent developments in the remotely-piloted aerial system (RPAS), as well as that in the structure-from-motion multi-
30   view (SfM-MVS) photogrammetry, have enabled effective acquisition of high-resolution topographic and imagery data (e.g., Westoby et al., 2012; Fonstad et al., 2013; Obanawa et al., 2014; Hayakawa et al., 2016). Such detailed earth surface data are useful for detailed topographic analysis, including topographic feature extraction and landform classifications, for areas of approximately 0.1–10 km^2 that cannot be achieved by low-resolution data of satellite imagery (e.g., Koarai et al., 2008). Moreover, although aerial photographs have often been utilized to investigate topographic features of DADs in such area and
35   scale (Siebert, 1984; Glicken, 1996; Yoshida and Sugai, 2007, 2012), high-quality stereo-paired aerial photographs are often unavailable in many areas over the world. The on-site acquisition of high-resolution topographic and imagery data using RPAS is also highly advantageous regarding the cost efficiency.

Based on the combined approaches of RPAS- and satellite-derived topographic data, here we perform detailed morphological analyses of a DAD in the north-eastern flank of Mt. Erciyes in Kayseri, central Turkey. The DAD of this area
40   has been described in a geological study of the Mt. Erciyes volcano (Şen et al., 2003), but details of the DAD have not yet been examined. We utilize an RPAS approach, which enables the acquisition and analysis of detailed, high-resolution morphological data for the hummocks formed on the DAD. We also utilize the medium-resolution topographic data (10 m DEM) derived from satellite SAR imagery (ALOS PRISM) for the analysis of a wider area. In particular, the volume of the

DAD has not been known but crucial for the clarification of the sector collapse event. Because it is hard to know from the deposits whose extent and depth have not been fully investigated, we examine the volume of the collapse by reconstructing the original topography of its source area, whose surrounding topography is well preserved.

2 Study area

5 Mt. Erciyes, located in the south of Kayseri City in central Turkey (Fig. 1), is the highest stratovolcano in this region with an elevation of 3917 m at its summit. The current mountain body of the volcano has been formed after the pre-Erciyes volcanic activities terminated about 3 Ma with an extensive ignimbrite eruption (Innocenti et al., 1975; Şen et al., 2003). The stratigraphy of Mt. Erciyes comprise basaltic, andesite, and dacitic lava flows in ca. 2.5–0.2 Ma, followed by pumice and pyroclastic flow deposits (Şen et al., 2003).

10 Among this stratigraphy, the DAD is described as the youngest deposits. Although the exact age is unknown, the sector collapse of this DAD is supposed to have occurred after 83 ka (Şen et al., 2003). Also, moraines formed in the last glacial maximum (21.3 ka) are present within the valley of the sector collapse (Üçker Valley, A in Fig. 1) (Sarıkaya et al., 2009). The sector collapse is therefore supposed to have occurred in 20–80 ka.

The DAD distribution has been recognized in 2–9 km downstream along a fluvial valley from the mountain top, with an
15 area of ca. 14 km^2 (Şen et al., 2003) (B in Fig. 1). The exact location of the downstream extent of the deposits is, however, hard to identify in the field due to the limited presence of outcrops, as well as to the possible erosion and rework of the deposits after its placement particularly in the fluvial valley. Nevertheless, we found several outcrops of the DAD along a newly constructed highway, whose locations are shown as stars in Fig. 1. The farthest outcrop is found to be 16 km away from the summit of Mt. Erciyes. Moreover, as noted later, hummocks of the DAD appear in 11–13 km downstream from the
20 summit. These indicate that the potential extent of the DAD is much more downstream over the area mapped by Şen et al. (2003), with an area of no less than 20 km^2.

The original flow direction of the debris avalanche is supposed to be eastward, as the main scar of the sector collapse faces east (A in Fig. 1; Fig. 2a). The flow then turned to the north, after blocked by the pre-existing slopes of the former caldera walls. The lake, located in the south of the bend of the DAD, can be a part of the remnant of the dammed lake by the
25 debris avalanche (D in Fig. 1), but the present lake is artificially modified to work as a reservoir.

Hummocks, characteristic mound-shaped topographic features of DADs, are densely and only found in an approximately 2 km^2 area around 11–13 km (along-valley distance) from the summit of Mt. Erciyes. Our topographic measurements, therefore, focus on this domain. As noted, this domain of hummocks is out of the range of the DAD area previously reported (B in Fig. 1; Şen et al., 2003), but the potential extent of the DAD likely covers this domain to the farther
30 downstream. However, as far as we investigate, no hummock is observed in other areas of the DAD along the valley. Some mound-shaped features on the eastern side of the DAD (C in Fig. 1) were found to be basaltic or andesite lava domes, as confirmed in the field.

A left-lateral strike slip fault, named as the Erciyes Fault as a member of the Ecemiş Fault group of the East Anatolian Fault zone, is mapped to potentially cut across the Mt. Erciyes in the northern-northeast to the southern-southwest direction
35 (Emre et al., 2011). The age and history of the fault activity are not well known.

The climate in the area is warm and dry, with an annual precipitation of ca. 400 mm. Due to the dry climate, vegetation cover is sparse. Although there have been climatic fluctuations including relatively wet periods in the late Pleistocene to Holocene, the climate has been dry enough not to grow dense vegetation since the last interglacial (Kuzucuoglu et al., 1999; Bayer Altin et al., 2015; Pickarski et al., 2015). Hence, the slope processes have not been so active to significantly modify
40 the topography, particularly in the dry periods. The original topography of the debris avalanche, as well as the landforms

Natural Hazards
and Earth System
Sciences

Discussions

surrounding the sector collapse, is therefore supposed to be well preserved, except for areas around valley bottoms where

fluvial or glacial modifications have been active and volcanic alluvial fans are well developed.
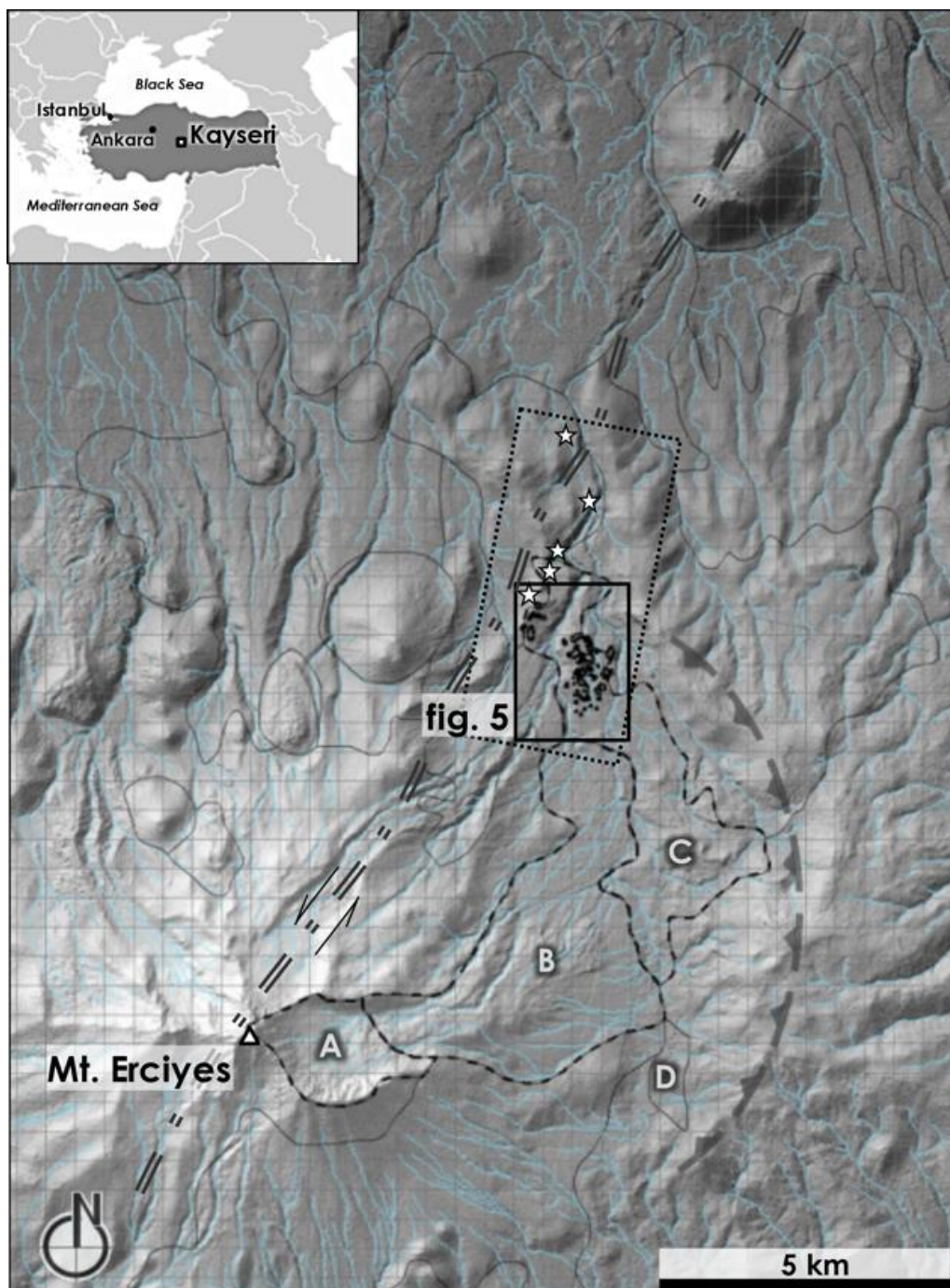

Figure 1: Map of the study area. Thin solid lines indicate the boundaries of lithological units reported by Şen et al. (2003). Units
5 **surrounded by dashed, solid lines show, from west to east, the sector collapse, DAD, and andesite lava domes, respectively. Stars**
locate outcrops of the DAD found in this study. Black solid lines within the extent of Figure 5 are the hummocks examined. Gray
dashed line with triangles indicates the remnant of caldera walls before the formation of modern Mt. Erciyes. Dashed double line
shows the approximate path of the Erciyes Fault mapped by Emre et al. (2011).

Natural Hazards
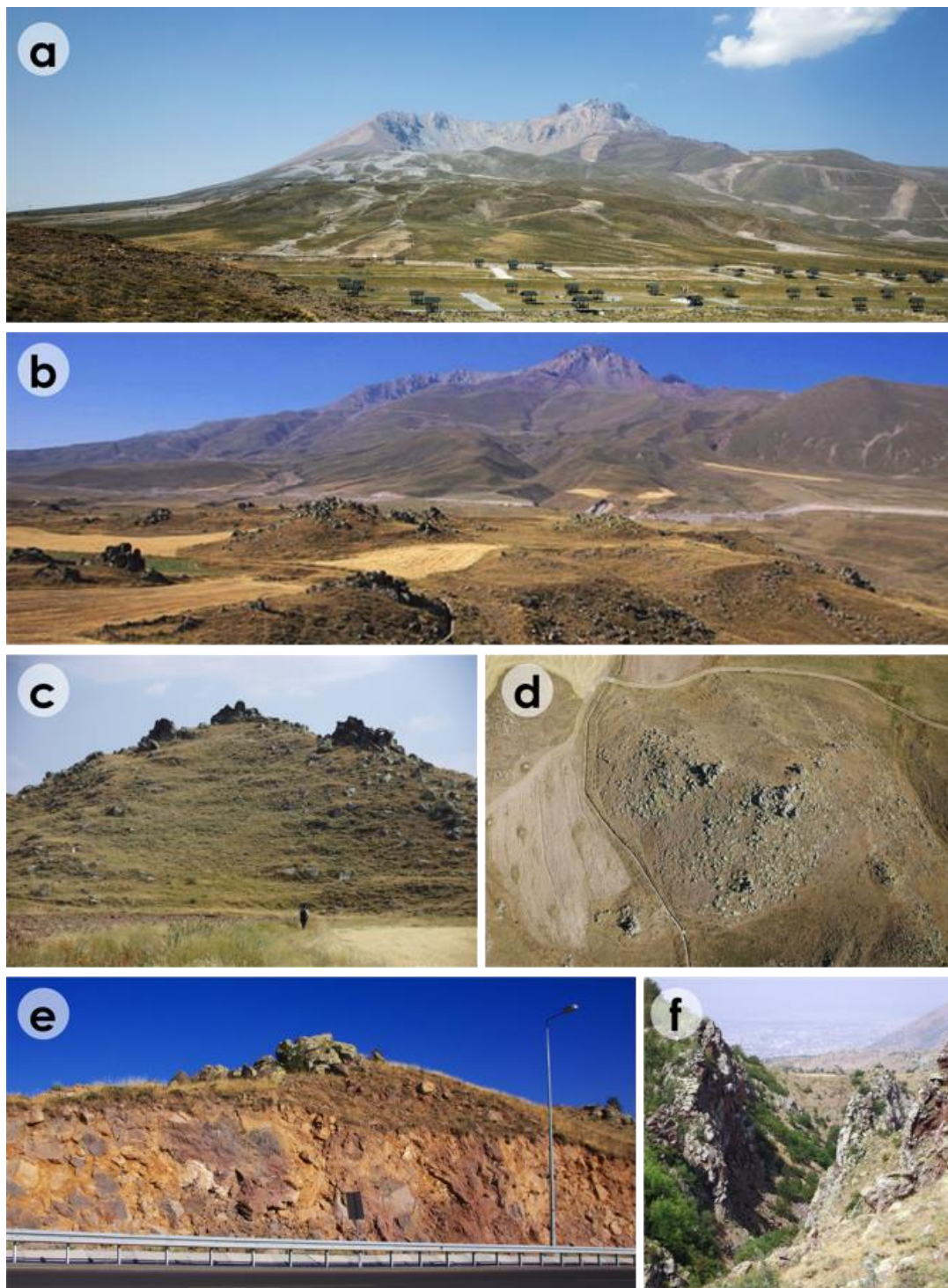and Earth System
Sciences
Open Access
Discussions
EGU

Figure 2: Pictures of the study area. Locations of these photos are shown in Figure 1. (a) The collapsed side of Mt. Erciyes (looking westward). The foreground area is the DAD, changing its flow direction from east to the north (right side) (b) Mt. Erciyes and the DAD on which hummocks are well preserved. (c) Ground-based view of a hummock on the DAD, approximately 30 m high. (d)

Aerial view of the hummock of b, taken by UAV. The diameter is approximately 150 m. (e) Outcrop of a hummock DAD along the highway. (f) Downstream view of the deeply-incised gorge just below the hummock-dominated area.

3 Methods

5   #### 3.1 RPAS-based SfM-MVS photogrammetry and hummock mapping

To measure the detailed surface morphology of the DAD, we apply the SfM-MVS photogrammetry using low-altitude aerial photographs taken by an RPAS. The RPAS, including a small unmanned aerial vehicle (UAV) equipped with a digital camera, enables to obtain low-altitude aerial photographs in the field. The image data obtained are used to capture the data of earth surface condition and morphology in a relatively broad area, typically for 0.1–10 km^2. We used two UAVs for the

10   measurement: DJI Phantom 2 on which a digital camera of Nikon Coolpix A (sensor resolution: 4928 × 3264 pixels, 35-mm equivalent focal length: 28 mm) or RICOH GR (sensor resolution: 4928 × 3264 pixels, 35-mm equivalent focal length: 28 mm) is mounted, and DJI Phantom 3 Professional with a built-in stabilized camera FC300X (sensor resolution: 4000 × 3000 pixels, 35-mm equivalent focal length: 20 mm).

In the field, we carried out the flights of the UAVs from several locations relatively high in elevation in and around the

15   area where hummocks are densely present. The UAVs were manually operated, and the flight courses were successively set to cover the area of interest sufficiently. During the flights, the camera shutter is set to work automatically at an interval of 2 seconds. One flight took ca. 10-20 minutes so that 300–600 of aerial photographs were taken for each flight.

Geographical coordinates of several ground control points (GCP) were also obtained, using a post-processed kinematic global navigation satellite system (GNSS) receiver. Trimble GeoExplorer 6000XH was used as the GNSS rover, whose log

20   data are corrected using the fixed GNSS base station of the International GNSS Service (IGS) network. The GCPs were placed in the main target area around the hummocks. Characteristic objects that are readily identifiable in the aerial photographs were selected as such GCPs, including intersections of roads, the flat stone surface at a small bridge, and large rock blocks with flat tops. The projection of the geographical coordinates is set to be the UTM zone 36N on WGS 84 (EPSG:32636).

25   Using hundreds of aerial photographs taken by the RPAS, we carry out the SfM-MVS photogrammetry. The photogrammetric software used is PhotoScan Professional Edition by Agisoft LLC. From the multiple photographs, the SfM process provides three-dimensional positions of the stereo-paired photographs, in which the same features are identified among the paired photographs as tie points. Although geographical coordinates of the camera locations can be known from the GNSS records in the built-in camera of the UAV devices, the positional accuracies of the single-source GNSS receiver of

30   the UAVs are low, being on the order of meters. The GCPs whose coordinates are obtained by the post-processed GNSS receiver are therefore placed in the image data to achieve better positional accuracies. The tie point cloud is adjusted to fit the GCPs, and the points with large reprojection errors (≥1.0) are removed. By the MVS-photogrammetric process, denser three-dimensional points are then further obtained from the aligned and paired images. Based on the resultant point density and ground resolution of the images, the resolution of the raster data including a DEM and an orthorectified composite image

35   are determined.

Using the DEM, orthorectified image, and DEM-derived slope distribution and topographic contour lines, the extent of each hummock on the DAD surface was traced using GIS software (ArcGIS Desktop 10.3 by ESRI). The detailed procedures are as follows: First, to identify local convex mounds in the DEM, the elevation values are multiplied by -1 to generate a flip-side of the DEM, and the local depression in the inverse surface are highlighted by applying the sink-fill

40   process. For the sink-fill, the D8 flow directions based on the surrounding eight cells are derived from the flip-side DEM (Jenson and Domingue, 1988), and the depressions are virtually filled up to match with the local trend surface. The filled

areas roughly correspond to the local mounds in the original DEM. Second, the orthorectified ground-surface image and slope distribution are used to detect the boundaries of the actual mounds. Because the flat lands in the main area are mostly cultivated whereas the mounds of hummocks are unsuitable for cultivation due to their rocky composition, the boundaries of the hummock mounds are clearly shown in the ground-surface images. Also, the gap of slope angles is also clear to separate

5   the mounds and surrounding flatlands. Topographic contour lines are supportively used to trace the mound boundaries, although the boundaries are not always horizontal and the contour lines themselves do not generally follow the mound boundaries except very flat areas. Polygon vector data showing the hummock mound boundaries are then obtained. The reliability of the mound boundaries was also checked in the field for some of the hummocks.

The geometric features of the hummocks are then examined in GIS. The area is readily calculated for each polygon.

10   The height of a hummock is estimated by constructing a flat basement surface of each hummock by linearly interpolating the elevation values on the polygon peripherals by triangular irregular network (TIN) surface. The maximum difference between the actual surface and the estimated basement surface is regarded as the height of the hummock. Although the actual mass of a hummock should exist in the underground areas, the depth of such the submerged structure is hard to be known, and the surficial height of hummocks have often been utilized as a geometrical index (Glicken, 1996). The upper-half volume of a

15   hummock, i.e., the volume of the hummock mound above the basement surface, is also obtained as one of the proximal indicators of the hummock size. The volume is calculated as the sum of the elevation differences between the actual surface and the estimated basement surface for each cell in a hummock polygon.

Two directionality indices of the polygons are calculated based on their major axis. One is the direction from the north, and another is the displacement angle against the flow direction of DAD. Fig. 3 shows the definition of the displacement

20   angle of the major axis of a hummock: the angle between the main direction of the valley-filling DAD and the major axis (Yoshida, 2014). The main direction of the DAD in the study site is the north. The distance from the source along the valley, as explained later, is also assigned to the centroid of each polygon (Fig. 3).
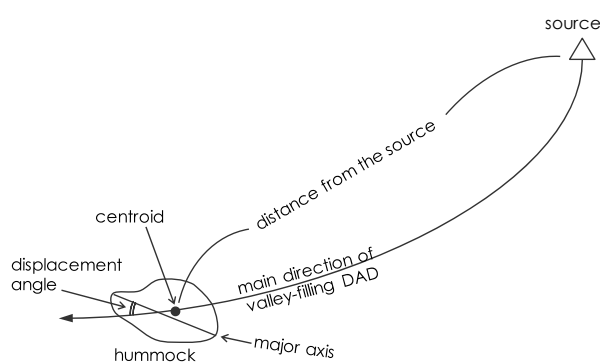
25   **Figure 3: Definition of the displacement angle of a hummock (modified after Yoshida, 2014).**

3.2. Reconstruction of the source area of DAD using PRISM-DEM

As a background data covering areas wider than the RPAS-derived data, we use satellite-based remote sensing topographic and imagery data by sensors of AVNIR-2 (Advanced Visible and Near Infrared Radiometer type 2) and PRISM

30   (Panchromatic Remote-sensing Instrument for Stereo Mapping), which were mounted on the satellite ALOS (Advanced Land Observation Satellite). The AVNIR-2 sensor has four bands for visible and near-infrared wavelengths, with a typical resolution is 10 m. Although this satellite imagery data is too coarse to be utilized as the data source for the extraction of hummocks in the study area, it can be used as a background image that cannot be fully covered by the RPAS-derived

images. The AVNIR-2 data was just used to check the presence of hummocky landforms in and around the DAD. The PRISM optical sensor is a panchromatic radiometer for wavelengths of 0.52–0.77 µm, with a spatial resolution of 2.5 m. The original data was processed to provide a DEM, whose resolution was originally 3 m but subtracted to 10 m resolution to avoid unexpected surficial noises. Although there remain more errors particularly around the borders of mosaic images due to their mismatching, the DEM can be used as a background topographic condition covering the whole area of the sector collapse, DAD, and surrounding areas. The resolution and accuracy of the DEM are, however, unsuitable for the extraction of small hummocks.

The PRISM-DEM was further processed to show topographic characteristics in the study site. The distances along flow paths based on the D8 flow directions are generated using the hydrological toolset in the GIS software, providing the position of the hummocks (the distance from the source) based on the flow directions (Fig. 3). The longitudinal and transverse profiles along the main course of the DAD are also obtained from the PRISM-DEM. Elevation and distance from the source (the summit of Mt. Erciyes) are sampled at a 100-m interval along the main course of the debris avalanche for the longitudinal profile. At the same time, the maximum elevation within a 500-m length of a transverse cross section perpendicular to the flow direction is recorded for each sampling point to represent the amount of reliefs along the valley bottom. Stream gradients at different scales are calculated from the sampled elevation by averaging for 400-m and 2,000-m horizontal lengths. The 400-m scale stream gradient represents local fluctuations in the longitudinal profile, while the 2,000-m gradient reflects the trend of elevation changes along the profile. Transverse cross profiles (3,000-m long) perpendicular to the flow direction are extracted at every 1,500 m along the main course of the debris avalanche.

The original surface of mountain slopes before the sector collapse is estimated based on the shape of the surrounding slopes, supposing that the topography has not been highly modified. For this purpose, two different approaches are applied: One is a simple linear extrapolation of the original slopes in a cross profile on both sides of the sector collapse, and the other is to fit a Bézier curve to the linearly extrapolated cross profile. The linear extrapolation may result in an overestimate of the original surface, while the Bézier curve fitting may result in an underestimate. The original surface may fall within these two different reconstructions. For the linear extrapolation, the cross-section points on the surrounding slopes just behind the scars which are supposed to preserve the original topography are used as the source. The length of the cross sections for the linear fitting is defined as ~400 m, according to the linearly of the slope cross sections. The extrapolated two lines over the collapsed area from the both sides of the scar (P_0 and P_2 in Fig. 4) cross at a certain point (P_1 in Fig. 4), which is regarded as the ridge of the reconstructed original slopes.

For the quadratic Bézier curve fitting, the edge points of the surrounding slopes on both sides of the collapsed area (P_0 and P_2) are used as the endmost control points, while the intermediate control point (P_1) is given as the cross point of the two linearly-extrapolated lines (Fig. 4). The function of a quadratic Bézier curve is given as:

$$B(t) = (1-t)[(1-t)P_0 + tP_1] + t[(1-t)P_1 + tP_2] \,, \tag{1}$$

hence

$$B(t) = (1-t)^2 P_0 + 2(1-t)tP_1 + t^2 P_2 \,, \tag{2}$$

where $B(t)$ is the estimated elevation, and t represents the relative position between the points of P_0 and P_2 ($0 \le t \le 1$). Eq. (2) was applied to the multiple transverse profiles across the collapsed area (A in Fig. 1), which are set at a horizontal interval of 300 m.

From the reconstructed cross profiles by the linear and Bézier methods, the original surfaces of the missing mountain body are derived using 3-dimensional TIN models. The differences between the reconstructed TIN surface and the present land surface are calculated as the estimated volumes of the sector collapse.
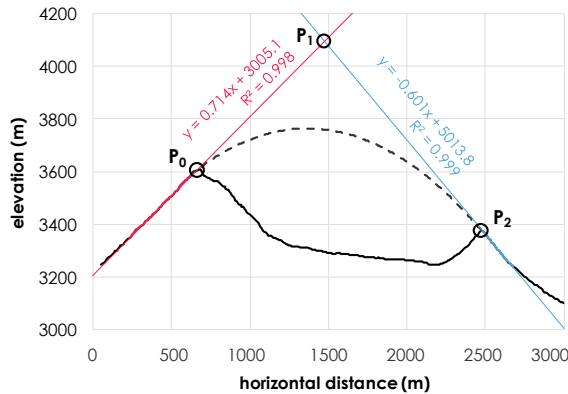
Figure 4: An example of reconstructing the original topographic surface of the sector collapse by two methods: linear extrapolation (solid red and blue lines) and Bézier curve fitting (dashed line).

4 Results

4.1 Morphometric characteristics and distribution of hummocks

The total number of UAV flights was 8 times, during which 2900 photos were taken. After excluding low-quality images and those with large errors in alignments, 1572 photos were successfully aligned and used for the photogrammetry. To adjust the geographical coordinates of the tie points and camera locations, GCPs were set in the images and the tie points and camera locations were adjusted to fit to the GCP-derived coordinates. In the field, 5 GCPs were set around the main area with hummocks, whose geographical coordinates taken by the post-processed GNSS provided positional errors of 0.48 m and 0.99 m in horizontal and vertical directions, respectively. Although the number of GCPs is not many, and the errors are on the order of decimeters, these error values are assumed to be sufficiently good for the analysis of hummocks in 10^1–10^3 m^2 scales. After removing the points with large reprojection errors (>0.79 pixels), the number of valid tie points for the paired images was 14,220,242. The multi-view stereo photogrammetry was then performed to generate the dense point cloud of 51,505,810. Based on this three-dimensional point cloud and the original images, the data of land surface imagery and topography were obtained, covering an area of 8.5 km^2. The resolution of the raster-type topographic data (DEM) was set to be 36 cm, based on the average point density of 7.8 pts/m^2. The orthorectified image was given with a resolution of 9.0 cm, based on the average ground resolution of the original image of 8.96 cm/pix.

Following the procedure described in the method, the outline of hummocks was extracted from the RPAS-derived DEM and orthorectified image (Figure 5). The number of the hummocks extracted was 65, all of which are, as noted, located approximately 11 to 13 km away from the DAD source (summit of Mt. Erciyes), and no other hummocks were identified.

Table 1 shows the basic morphological properties of the hummocks. The polygon area ranges over two orders of magnitude from 100 m^2 to 20,000 m^2, with a mean area of 3315.8 m^2. The height shows less variation from 1 to 20 m with a mean of 5.4 m, while the volume largely ranges from 200 to 770,000 m^3 with a mean of 79,429 m^3. The lengths of major and minor axes are tens to hundreds of meters with means of 69.1 m and 41.4 m, respectively. The mean elongation ratio, i.e., the length ratio of the major axis to the minor axis, is 1.7, equivalent to an approximate aspect of 5:3.

The displacement angle (the relative orientation against the flow direction of the debris avalanche) almost fully ranges from 0° to 90°, with an average of 38.1°. Fig. 6 shows more details of the orientation and displacement of the hummocks in histograms. The north-based orientation shows large fraction toward the north (Fig. 6a), while the displacement angle shows a bimodal distribution in the histogram, with relatively large fraction around 0–40° (Fig. 6b). These indicate that many hummocks tend to follow the direction of the northward flow of the debris avalanche, but some are exceptionally placed with large displacements against the flow direction.

Natural Hazards
and Earth System
Sciences

Discussions

Open Access
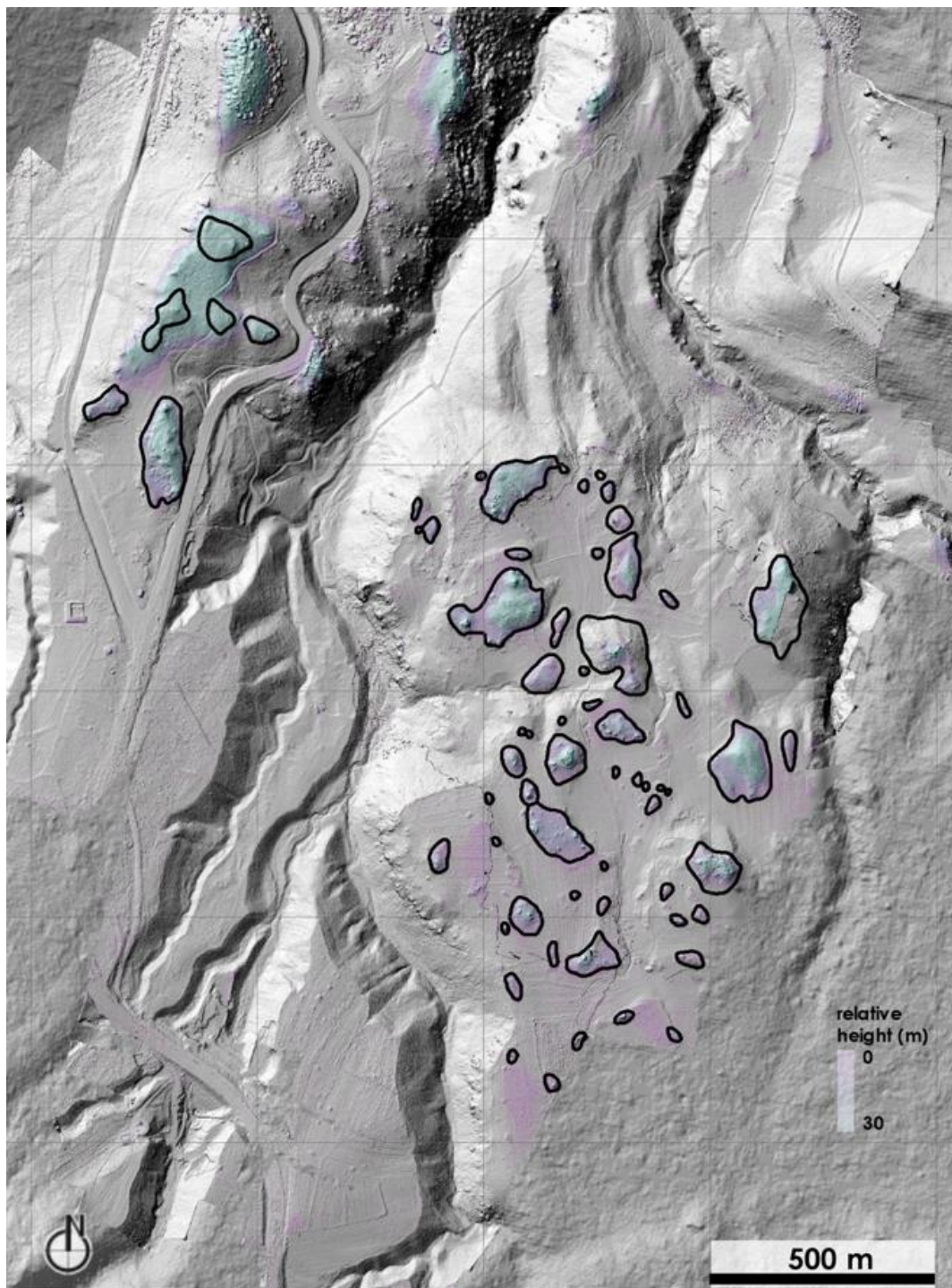
Figure 5: Map of the hummocks extracted in the study area (n = 65). Blue to purple colors show the sink-filled areas on the inverse DEM, indicating the locations of local mounds and ridges. Black solid lines represent the mound boundaries of hummocks identified. Note that not all the sink-filled areas are identified as hummocks, based on the interpretation of orthorectified images and field observations. Hillshade images are derived from RPAS-derived 36-cm DEM (foreground) and 10-m PRISM-DEM (background).

Table 1: Morphological properties of hummocks

properties of hummocks	average	minimum	maximum
distance from the source (m)	12,177	11,158	13,464
area (m^2)	3,315.8	118.3	19,615.6
top height (m)	5.4	0.9	20.1
volume (m^3)	79,429	210	774,506
major axis length (m)	69.1	13.7	240.5
minor axis length (m)	41.4	11.5	140.5
elongation ratio	1.7	1.0	3.1
displacement angle (degrees)	38.1	0.3	89.6
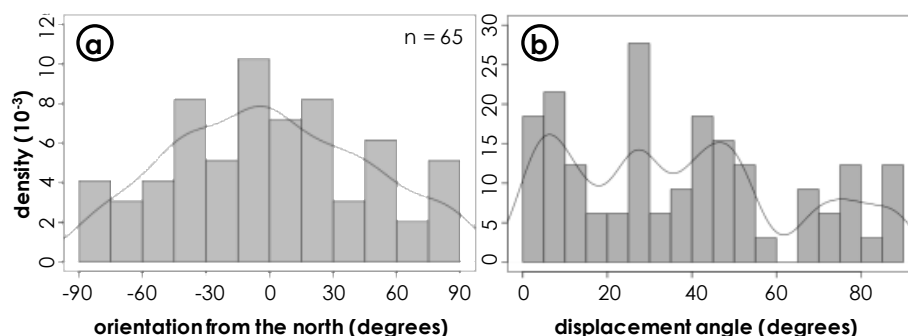
Figure 6: Horizontal angles of the direction of hummocks. (a) Orientation from the north. West is -90° and east is 90°. (b) Displacement angle in 0–90°.

Fig. 7 shows the longitudinal profile and stream gradients along the main course of the DAD derived from PRISM-DEM. The longitudinal traces of maximum elevation within 500 m from the valley center are also shown as a gray line. The differences of the maximum elevation and the bottom elevation indicate deepness of the incision in the valley bottom. With some fluctuations, both the local and trend stream gradients decrease as the distance from the source increase. The gradients are particularly low in the reach upstream of the portion where hummocks are present (around 8–12 km from the source). In this upstream reach within the caldera wall, less difference in elevations is observed for the valley bottom and nearby 500-m cross section area, representing the low relief along the stream. In contrast, the stream gradients, as well as the elevation differences, are particularly high in the downstream reach of the hummock-dominated area for approximately 5 km (13–18 km from the source). In this reach, the trend stream gradient (2,000-m scale) increases up to 0.1 m/m, while the elevation difference reaches 100–200 m. This reach corresponds to the outlet of the caldera and shows a form of the deep gorge (Fig. 2f). This can be regarded as a knickzone, which has relatively steeper gradient than the adjacent upstream and downstream reaches (Hayakawa and Oguchi, 2006).

Natural Hazards
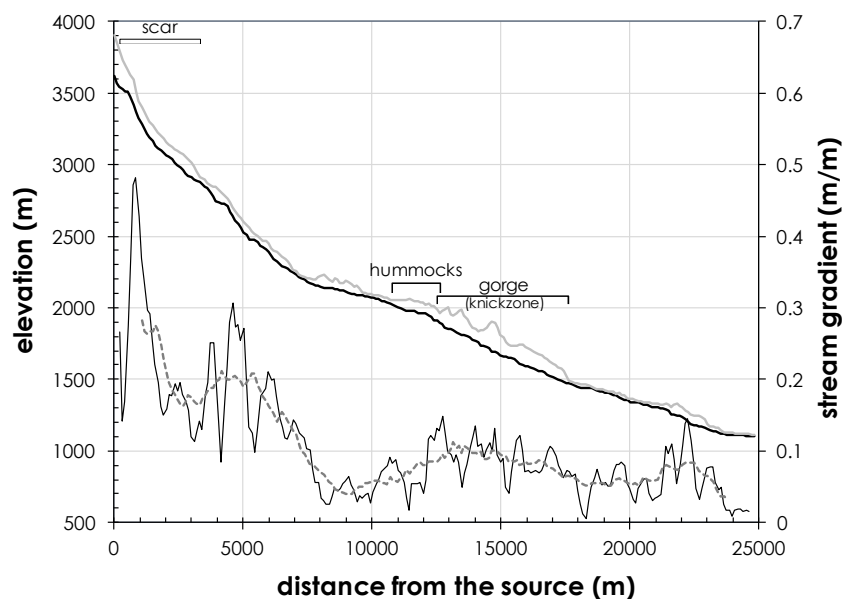and Earth System
Sciences
Discussions

Open Access

Figure 7: Longitudinal profile and stream gradient along the main course of the DAD. The black solid line in the upper side (left y-axis) indicates the longitudinal profile along the main course whose location is shown in Figure 1, while the solid gray line indicates the maximum elevation within the 500-m range across the main course. The thin black line on the lower side (right y-axis) is the
5   **stream gradient averaged for 400-m reach upstream and downstream for each sampling point, whereas the dashed gray line is that averaged for 2000-m reach.**

      Transverse cross profiles along the DAD extracted from PRISM-DEM show downstream widening of the DAD in elevations of 2800–2200 m, and narrowing in 2200–1600 m (Fig. 8). The potential extent of the DAD, whose downstream
10   limit corresponds to the location of the northernmost outcrop identified in the field (Fig. 1), was highlighted as black solid lines in Fig. 8. The upper part of the DAD (approximately 2800–2300 m in elevation) shows convex-up cross profiles, whereas the middle part (2300–2000 m) is more straight and flat. The downstream-most part (below 2000 m) exhibits more rugged shape by the incised valley of the knickzone reach. The hummocks are located in the transitional area (around 2000 m elevation) from the flat to the incised areas. Far downstream areas out of the potential DAD extent again show straight and
15   flat transverse profiles.

Natural Hazards
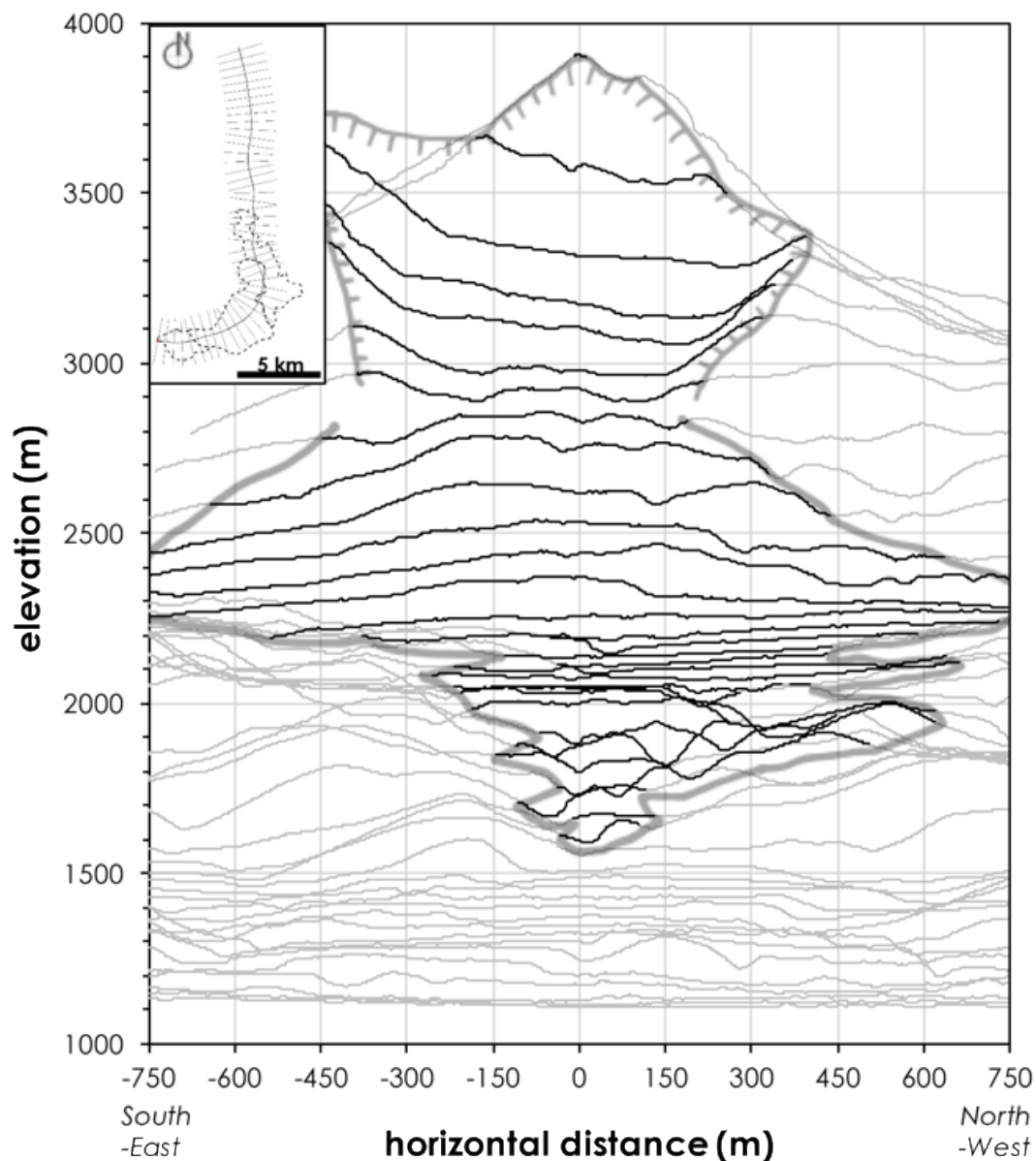and Earth System
Sciences
Discussions

Figure 8: Transverse profiles across the DAD. Areas of the sector collapse and the potential DAD extent are shown in black surrounded by thick gray lines. Inset map (upper left) shows the location of these sections along the main course of the debris avalanche over the mapped extent of the DAD.

5

The area of the polygons of the hummocks was summarized for each 500-m bin of the distance from the source summit to be compared with the previously reported binned average of hummock areas along the distance (Fig. 9; Yoshida et al., 2012). In Fig. 9, the mean area of all hummocks identified for each 500-m distance is shown as white circles, whereas the mean area for all the hummocks is shown as a black horizontal bar. Due to the limited distribution of the hummocks

10 concentrated in the area of 11–13 km from the summit, the distance-size relationship of the Erciyes case does not follow those in the previous studies, and even the downstream increase in the hummock area is observed.
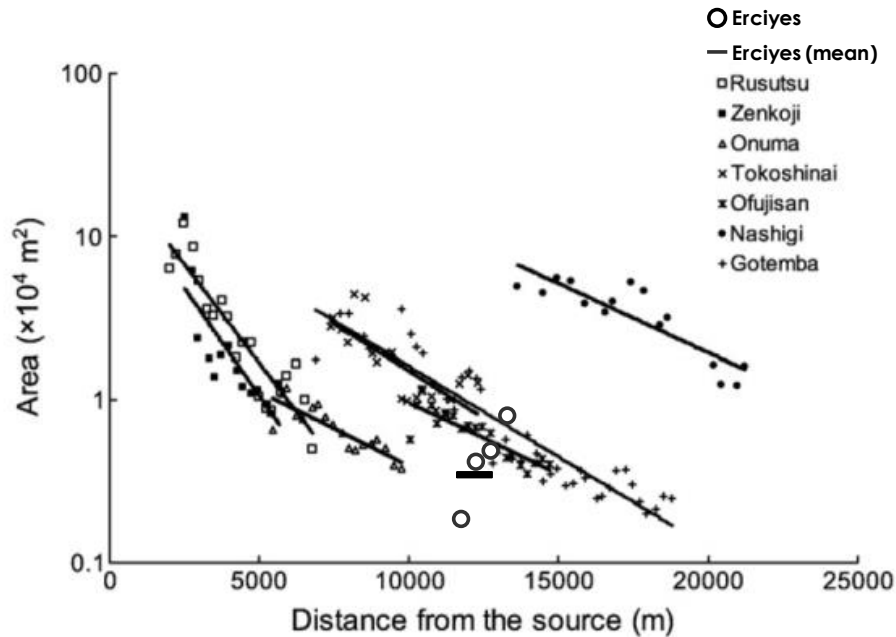
Figure 9: Relationship between the distance from the source and hummock size for the avalanche in Mt. Erciyes and those previously reported by Yoshida et al. (2012). The white circles indicate the mean area of hummock polygons summarized for each 500-m bin of the distance, while the black horizontal bar shows the average areas for all the hummocks in Erciyes. Solid lines are linear regressions for each avalanche previously reported.

4.2 Volume estimation of DAD by the source area reconstruction

Using the two different interpolation methods by linear and Bézier, the original surfaces of the mountain body before the sector collapse were reconstructed (Figs. 10, 11). The particular difference between the linear and Bézier methods is the maximum summit elevation of the reconstructed surface. The summit of the linearly interpolated original mountain body reaches 4100 m of elevation that is much higher than the present summit of 3917 m (Fig. 10c), while that by the Bézier method do not exceed the present summit elevation (Fig. 10d). In any case, the summit of the reconstructed mountain body appears at 1 km southeast of the current summit (Figs. 10a, b, 11b, c).

The volume of the missing mountain body by the sector collapse is calculated as the sum of the elevation differences between the reconstructed surface and the present landform: 12.75×10^8 m^3 by the linear method, and 10.67×10^8 m^3 by the Bézier method. Due to the preexisting dissection of the mountain before the collapse or a crater on the top, this reconstructed volume may be reduced by approximately 10% (Aramaki, 1963; Yonechi et al., 1988; Yoshida and Sugai, 2007). If this is applied, the estimated source volume of the sector collapse is given as 9.60–11.48×10^8 m^3. Since the plan area of the sector collapse source area is 5.2 km^2, the mean depth of the missing mountain body is obtained to be 186–223 m.
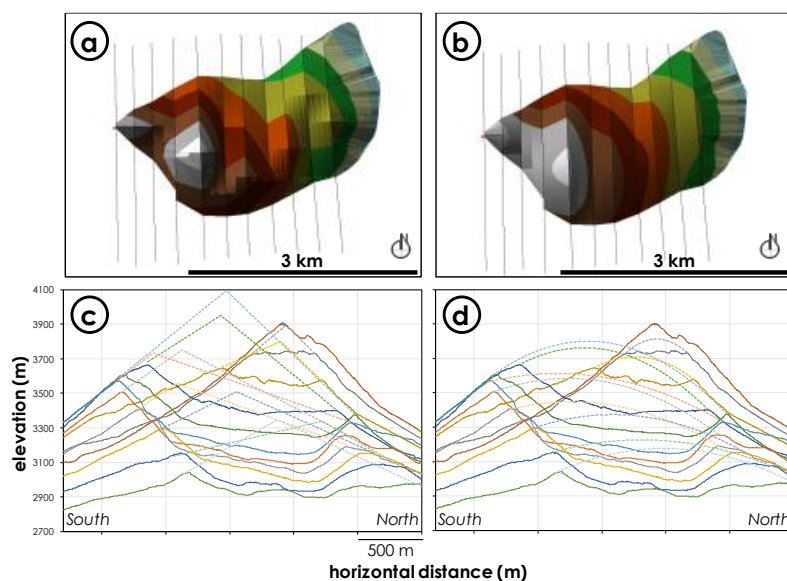
Figure 10: Reconstruction of the source area of the sector collapse. (a) Plan view of the reconstructed surface by the linear method. The red triangle indicates the location of the current summit of Mt. Erciyes. (b) Plan view of the reconstructed surface by the Bézier method. (c) Transverse profiles of the original surface by the linear extrapolations. (d) Transverse profiles by Bézier curve fitting.
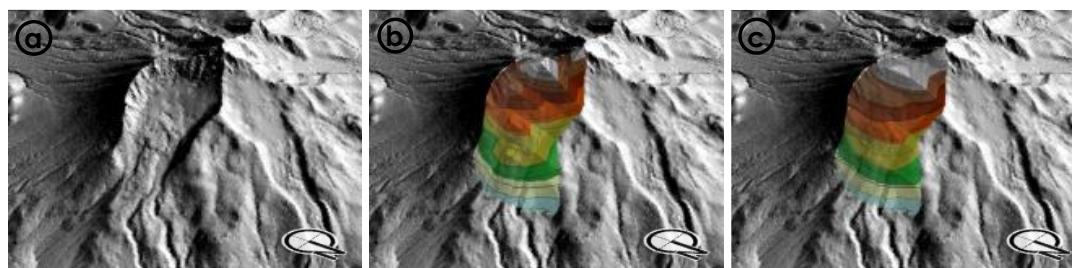

Figure 11: Bird-eye views of the reconstructed source area of the sector collapse. (a) Present topography of the scar. (b) 3D TIN of reconstructed surface of the original mountain body by linear extrapolations. (c) 3D TIN of reconstructed surface of the original mountain body by Bézier curve fitting.

5 Discussion

5.1 Characteristics of the debris avalanche inferred from the volume and thickness

Because of the expansion of the original mass and sediment entrainment during the transport, the volume of DAD may be larger than that of the missing sector for 25–30% (Siebert, 1984; Yoshida and Sugai, 2007). Accounting for the estimated source volume of $9.6–11.5 \times 10^8$ m³, the potential volume of the DAD would become $12–15 \times 10^8$ m³. This estimated volume is relatively larger than the average volume (ca. 5×10^8 m³) of reported DADs in the Holocene and Pleistocene (Siebert, 1984), but falls within the range of $2–260 \times 10^8$ m³ (Siebert, 1984). If compared with the known cases, the estimated volume is comparable to the debris avalanche in the historical time period at Mt. Iriga in the Philippines, whose volume is known as 15×10^8 m³ (Aguila et al., 1986; Paguican et al., 2012), and more than half of that of the Mt. St. Helens case in 1980 as $25–28 \times 10^8$ m³ (Voight et al., 1983; Siebert et al., 1987; Glicken, 1996). Also, the estimated volume of Erciyes is approximately twice or three times of the well-described case of the northern flank of Mt. Bandai (Japan) in 1888

triggered by a phreatic eruption (4.9×10^8 m^3) (Yonechi et al., 1988; Yonechi and Chiba, 1989; Yoshida, 2012), or the non-eruptive case of Mt. Unzen-Mayuyama (Japan) in 1792 (4.4×10^8 m^3) (Inoue, 1999; Takarada and Melendez, 2006).

Although the exact extent of the DAD is hard to be clarified in this study, the roughly-estimated potential extent of the DAD identified in this study has an area of at least 20 km^2, which is apparently larger than that (14 km^2) previously mapped

5   (Şen et al., 2003). Dividing the estimated source volume of the DAD (12–15×10^8 m^3) by the potential extent of the depositional area (20 km^2), the mean thickness of the DAD is roughly obtained to be 60–75 m. This thickness of DAD is much larger than those reported in the previous studies: e.g., 25–30 m for Mt. Asama (Yoshida and Sugai, 2010), 45 m for Mt. St. Helens (Voight et al., 1983). The area and volume of the DADs across the world summarized by Siebert (1984) also gives an average thickness of 24 m with a range of 3–58 m, and the DAD thickness for Mt. Erciyes is out of the range of the

10   reported ones. This supports that the potential extent of the depositional area of the DAD of Mt. Erciyes can be much larger than 20 km^2, potentially twice to three-times of the identified area. Although the sedimentary evidence is not available in the downstream areas, the debris avalanche could have flown down over the gorge, and spread over the relatively flat area farther than 18 km from the source summit (Fig. 7) with the elevation lower than ca. 1500 m (Fig. 8).

5.2 Debris avalanche and formation of hummocks

15   Judging from the limited number of plots in Fig. 9, the distance-size of the observed hummocks in Erciyes may be comparable to the case of the Onuma avalanche on Komagatake volcano, the Ofujisan avalanche on Nasu volcano, or the Gotenba debris avalanche on Mt. Fuji (Yoshida et al., 2012). However, unlike the other cases, hummocks are densely found only in a limited area (11–13 km from the source), and the distance-size relationship of hummocks cannot be directly compared to the other cases in which hummocks are more evenly distributed (Siebert, 1984; Yoshida et al., 2012).

20   In turn, the absence of hummocks in both upstream and downstream reaches indicate a different pattern of debris avalanche flow for this particular case of Mt. Erciyes. It should be noted that the distributions of the DAD and hummocks seem to be affected by the presence of the caldera wall (Fig. 1). Hummocks in DADs are primarily formed due to the initial stage of sliding of the original sector of the mountain body, and some of the blocks remain its original structure to appear as secondary hummocks by floating on the surface of DADs in the later stage (Paguican et al., 2014). The absence of such

25   primary hummocks on DADs may indicate either that hummocks are not formed due to the high fracturing of DADs, or that hummocks are formed but buried by subsequent sediment covering over the DAD. The presence of convex-up cross profiles in elevation of 2800–2300 m (Fig. 8, or around the letter B in Fig. 1) may indicate some post-collapse modifications and sediment deposition in this upstream area of the DAD. Although no significant eruptive activity, which may sufficiently cover the DAD surface with thick tephra or pyroclastic flows, has been recognized in the volcanic stratigraphy (Şen et al.,

30   2003), more local, post-collapse eruptive activities including pyroclastic flows might have occurred to cover the upper portion of the DAD. If this is the case, the existed primary hummocks could have been hidden by such the surficial sediment (Yoshida and Sugai, 2007). Also, from our field observations, outcrops showing the volcanic colluvial or alluvial deposits were partially found around this upstream area of the DAD, and sediment coverage of such loose materials after the collapse would be expected.

35   In the downstream reach of the present hummocks, the stream gradient is high, and the valley width is narrow forming a knickzone (Figs. 7, 8). This topographic feature could have existed before the sector collapse because this location corresponds to the intersection of the north-oriented valley, which seems to follow the mapped fault line as discussed later, and the former caldera wall of the pre-Erciyes volcanic activity (Fig. 1). The debris avalanche is supposed to have flown to the north after its initial change in the direction blocked by and following the former caldera wall in the east (Fig. 1) and

40   went over the wall at this pre-existed narrow outlet valley. The flow could have rapidly spread over the relatively flat area within the caldera wall. In particular, the debris avalanche could have had low viscosity with high water content, if there had been sufficient ice of glaciers on the original mountain in the glacial period, likely under the cool and wet climate in the late

Pleistocene (Sarıkaya et al., 2009; Bayer Altin et al., 2015). At the entrance of this narrow outlet valley, however, the flow could have had a limited speed to enter the valley over the caldera wall. The secondary hummocks could have been once placed around this terminal portion within the caldera wall. The flow could then have acquired higher speed when flowing through the steepened reach of the knickzone. The bimodal distribution of the displacement angle of hummocks would

5 support this hypothesis (Fig. 6b). As suggested by the displacement angles, some hummocks with displaced orientations indicate a partial compressional regime of the debris avalanche, while the other, majority of hummocks without large displacements indicate an extensional regime of the debris avalanche due to the rapid northward flow through the valley (Paguican et al., 2014; Yoshida, 2014).

The debris avalanche materials which went over the gorge could have been further deformed and shallowly spread over

10 the relatively flat area after reaching the downstream of the knickzone (Figs. 7, 8). Hummocks may no longer be formed in such highly-fractured materials of the debris avalanche. As noted, no data on the detailed geological structure in the downstream areas is available, and it is hard to know the feasible extent of the DAD. Further careful investigations regarding the remnant of this DAD would be required to clarify the actual impact of the debris avalanche in this region.

5.3 Potential effects of fault lines on the debris avalanche

15 The presence of the strike-slip Erciyes Fault (Fig. 1) may also have affected the debris avalanche. Although the exact age and intensity of the fault activity are unknown, and the presence of the fault itself also needs further careful assessments (Okumura et al., 2016), the regional stress field related to this fault group could have affected the occurrence and the direction of the sector collapse of Mt. Erciyes. In general, sector collapses often occur in the direction perpendicular to the major horizontal compression by faulting beneath the volcano (Moriya, 1980; Siebert, 1984; Vidal and Merle, 2000; Tibaldi

20 et al. 2008), or in parallel to the fault directions (Lagmay et al., 2000; Yokoyama and Nakagaki, 2003; Wooler et al., 2009). In Mt. Erciyes, the major horizontal compression by the strike-slip faults in the north-south direction could have caused the sector collapse toward the east. Furthermore, the northward valley seems to have been formed along the fault line cutting the caldera wall. The debris avalanche, which has flown to the north after blocked by the pre-existed caldera wall, could have spread far downstream by overpassing the former caldera wall along the pre-existed valley. In such a case, the existence of

25 local faults has dual significances, in the occurrence of sector collapse itself, and in the directionality of the debris avalanche. Although further examinations of this issue are out of the scope of this study, detailed surveys of active faults and stress field in this region is also highly significant in predicting the future sector collapse of the volcano (Tibaldi et al. 2008; Wooler et al., 2009).

6 Conclusions

30 In this study, we utilized the RPAS-based SfM-MVS photogrammetry to map the topography of DAD of Mt. Erciyes, and detailed outlines of hummocks on the DAD were successfully extracted from the high-definition land surface data. Despite the limited availability of high-resolution aerial or satellite images, rapid on-site acquisition by RPAS-based SfM-MVS photogrammetry enabled to obtain new insights regarding the formation of hummocks and DAD by the sector collapse of Mt. Erciyes. Also, the volume of the sector collapse was estimated by reconstructing the original topography in the source

35 area. Although the precise extent of the DAD is hard to be known, the estimated volume of the DAD of $12–15 \times 10^8$ m^3 suggests that considerable amount of sediment could have spread far downstream over the known or observed limit of the present DAD extent. Morphological analysis of the extracted hummocks suggested that the geometry of the hummocks in this study area is characterized by pre-existing topographic constraints, which significantly controlled the dynamics of the debris avalanche and formation of hummocks. In particular, former caldera walls had a strong effect on the flow direction of

40 the debris avalanche, as well as its flow over the caldera walls. The presence of strike-slip fault might also have considerable

effects on both the occurrence of the sector collapse and the flow course of the debris avalanche. Such factors including pre-existing topographic and tectonic characteristics should carefully be examined for the hazard estimate in the case of sector collapse, which may occur in many places over the world.

The study area is one of the potentially hazardous areas in the East Anatolian Fault zone with densely distributed
5   volcanoes and faults. The detailed map of the DAD can be incorporated into a regional geomorphological map to be further examined together with other geomorphological features including fluvial valleys, terraces, lakes and active faults (Erol, 1999). Although the age of the sector collapse is not well known, possibly 20–80 ka (Şen et al., 2003; Sarıkaya et al., 2009) and needs to be further investigated, subsequent sediment supply from the DAD could have affected ancient human activities in the Holocene period in the downstream basin areas where a lot of archaeological sites are present (Kontani et al., 2014).
10   Investigations of the DAD and surrounding palaeoenvironments will provide further insights for the potential disaster and its mitigation in the study area, including floods, volcanism, landslides and fault-induced earthquakes.

References

Aguila, L. C., Newhall, C. G., Miller, C. D. and Listanco, E. L.: Reconnaissance geology of a large debris avalanche from Iriga volcano, Philippines, Philipp. J. Volcanol., 3, 54–72, 1986.

Aramaki, S.: Geology of Asama volcano, J. Fac. Sci. Univ. Tokyo, Sect. II, 14, 229–443, 1963.

20   Bayer Altin, T., El Ouahabi, M. and Fagel, N.: Environmental and climatic changes during the Pleistocene–Holocene in the Bor Plain, Central Anatolia, Turkey, Palaeogeogr. Palaeoclimatol. Palaeoecol., 440, 564–578, doi:10.1016/j.palaeo.2015.09.011, 2015.

Bernard, B., van Wyk de Vries, B., Barba, D., Leyrit, H., Robin, C., Alcaraz, S. and Samaniego, P.: The Chimborazo sector collapse and debris avalanche: Deposit characteristics as evidence of emplacement mechanisms, J. Volcanol.
25   Geotherm. Res., 176(1), 36–43, doi:10.1016/j.jvolgeores.2008.03.012, 2008.

Dufresne, A. and Davies, T. R.: Longitudinal ridges in mass movement deposits, Geomorphology, 105(3–4), 171–181, doi:10.1016/j.geomorph.2008.09.009, 2009.

Emre, Ö., Duman, T. Y., Özalp, S., Elmaci, H. and Olgun, S.: 1:250,000 Scale Active Fault Map Series of Turkey, Kayseri (NJ36-8) Quadrange, Ankara., 2011.

30   Erol, O.: A geomorphological study of the Sultansazliği lake, central Anatolia, Quat. Sci. Rev., 18(4–5), 647–657, doi:10.1016/S0277-3791(98)00102-4, 1999.

Fonstad, M. A., Dietrich, J. T., Courville, B. C., Jensen, J. L. and Carbonneau, P. E.: Topographic structure from motion: a new development in photogrammetric measurement, Earth Surf. Process. Landforms, 38(4), 421–430, doi:10.1002/esp.3366, 2013.

35   Glicken, H.: Rockslide-debris avalanche of may 18, 1980, Mount St. Helens volcano, Washington., 1996.

Hashimoto, N., Isoyama, K., Kuboki, J., Okumi, S. and Ozawa, A.: A geomorphological study of Iwaki volcano – particularly on the Akakurazawa mudflow hills (in Japanese with English abstract), Bull. Geol. Surv. Japan, 30, 369–377, 1979.

Hayakawa, Y. S. and Oguchi, T.: DEM-based identification of fluvial knickzones and its application to Japanese mountain
40   rivers, Geomorphology, 78, 90–106, doi:10.1016/j.geomorph.2006.01.018, 2006.

Hayakawa, Y. S., Obanawa, H., Saito, H. and Uchiyama, S.: Geomorphological applications of Structure-from-Motion Multi-View Stereo photogrammetry: A review (in Japanese with English abstract), Trans. Japanese Geomorphol. Union, 37(3), 321–343, 2016.

Hayakawa, Y. S., Yoshida, H., Dragut, L. and Oguchi, T.: Automated extraction of hummocks in debris avalanche deposits using DEMs: A case study at Mt. Gassan, northwest Japan, Zeitschrift für Geomorphol., doi:10.1127/zfg_suppl/2017/0361, *in press*.

Innocenti, F., Mazzuoli, R., Pasquarè, G., Radicati Di Brozolo, F. and Villari, L.: The Neogene calcalkaline volcanism of Central Anatolia: geochronological data on Kayseri—Nigde area, Geol. Mag., 112(4), 349, doi:10.1017/S0016756800046744, 1975.

Inoue, K.: Shimabara-Shigatusaku earthquake and topographic changes by Shimabara catastrophe in 1792 (in Japanese with English abstract), J. Japan Soc. Eros. Control Eng., 52(4), 59–69, 2000.

Jenson, S. K. and Domingue, J. O.: Extracting topographic structure from digital elevation data for geographic information system analysis, Photogramm. Eng. Remote Sensing, 54(11), 1593–1600, doi:0099-1112/88/5411-1593$02.25/0, 1988.

Koarai, M., Sato, H. P., Araiba, K., Osanai, N. and Itoh, H.: Geomorphological study of the Leyte debris avalanche using satellite imagery remote sensing (in Japanese with English abstract), J. Japan Landslide Soc., 45, 106–117, 2008.

Kontani, R., Sudo, H., Yamaguchi, Y., Hayakawa, Y. S. and Odaka, T.: An Archaeological Survey in the Vicinity of Kültepe, Kayseri Province, Turkey, in Current Research at Kültepe-Kanesh: An Interdisciplinary and Integrative Approach to Trade Networks, Internationalism, and Identity, edited by L. Atici, F. Kulakoğlu, G. Barjamovic, and A. Fairbairn, pp. 95–106, Lockwood Press, Atlanta, 2014.

Kuzucuoglu, C., Bertaux, J., Black, S., Denefle, M., Fontugne, M., Karabiyikoglu, M., Kashima, K., Limondin-Lozouet, N., Mouralis, D. and Orth, P.: Reconstruction of climatic changes during the Late Pleistocene, based on sediment records from the Konya Basin (Central Anatolia, Turkey), Geol. J., 34(1–2), 175–198, doi:10.1002/(sici)1099-1034(199901/06)34:1/2<175::aid-gj820>3.3.co;2-d, 1999.

Lagmay, A. M. F., van Wyk de Vries, B., Kerle, N. and Pyle, D. M.: Volcano instability induced by strike-slip faulting, Bull. Volcanol., 62(4–5), 331–346, doi:10.1007/s004450000103, 2000.

Mizuno, Y.: Geomorphology of Okinajima mud flow area, special reference to mud flow hills (in Japanese), Ann. Tohoku Geogr. Assoc., 11(1), 22–24, 1958.

Moriya, I.: "Bandaian Eruption" and landforms associated with it (in Japanese with English abstract), in Collection of articles in memory of retirement of Prof. K. Nishimura from Tohoku Univ., pp. 214–219., 1980.

Nakamura, Y.: Geology and petrology of Bandai and Nekoma volcanoes, Sci. Reports, TohokuUniversity, 3(14), 67–119, 1978.

Obanawa, H., Hayakawa, Y., Saito, H. and Gomez, C.: Comparison of DSMs derived from UAV-SfM method and terrestrial laser scanning (in Japanese with English abstract), J. Japan Soc. Photogramm. Remote Sens., 53(2), 67–74, doi:10.4287/jsprs.53.67, 2014.

Okumura, K., Hayakawa, Y. S., Kontani, R. and Kulakoglu, F.: Quaternary activity of the Erciyes Fault southeast of the Kayseri Basin, Turkey, in Abstracts, American Geophysical Union 2016 Fall Meeting, T41B–2918., 2016.

Orton, G. J.: Volcanic environments, in Sedimentary environments, edited by H. G. Reading, pp. 485–567, Blackwell Science., 1996.

Paguican, E. M. R., van Wyk de Vries, B. and Lagmay, A. M. F.: Volcano-tectonic controls and emplacement kinematics of the Iriga debris avalanches (Philippines), Bull. Volcanol., 74(9), 2067–2081, doi:10.1007/s00445-012-0652-7, 2012.

Paguican, E. M. R., van Wyk de Vries, B. and Lagmay, A. M. F.: Hummocks: how they form and how they evolve in rockslide-debris avalanches, Landslides, 11(1), 67–80, doi:10.1007/s10346-012-0368-y, 2014.

Pickarski, N., Kwiecien, O., Djamali, M. and Litt, T.: Vegetation and environmental changes during the last interglacial in eastern Anatolia (Turkey): A new high-resolution pollen record from Lake Van, Palaeogeogr. Palaeoclimatol. Palaeoecol., 435, 145–158, doi:10.1016/j.palaeo.2015.06.015, 2015.

Sarıkaya, M. A., Zreda, M. and Çiner, A.: Glaciations and paleoclimate of Mount Erciyes, central Turkey, since the Last Glacial Maximum, inferred from 36Cl cosmogenic dating and glacier modeling, Quat. Sci. Rev., 28(23–24), 2326–2341, doi:10.1016/j.quascirev.2009.04.015, 2009.

Şen, E., Kürkcüoglu, B., Aydar, E., Gourgaud, A. and Vincent, P. M.: Volcanological evolution of Mount Erciyes stratovolcano and origin of the Valibaba Tepe ignimbrite (Central Anatolia, Turkey), J. Volcanol. Geotherm. Res., 125(3–4), 225–246, doi:10.1016/S0377-0273(03)00110-0, 2003.

Shea, T. and van Wyk de Vries, B.: Structural analysis and analogue modeling of the kinematics and dynamics of rockslide avalanches, Geosphere, 4(4), 657, doi:10.1130/GES00131.1, 2008.

Siebert, L.: Large volcanic debris avalanches: Characteristics of source areas, deposits, and associated eruptions, J. Volcanol. Geotherm. Res., 22(3–4), 163–197, doi:10.1016/0377-0273(84)90002-7, 1984.

Siebert, L.: Threats from debris avalanches, Nature, 356(6371), 658–659, doi:10.1038/356658a0, 1992.

Siebert, L., Glicken, H. and Ui, T.: Volcanic hazards from Bezymianny- and Bandai-type eruptions, Bull. Volcanol., 49(1), 435–459, doi:10.1007/BF01046635, 1987.

Takarada, S. and Melendez, C.: Depositional features and transport mechanism of debris avalanches: the 1980 Mount St. Helens, Usu Zenkoji, and 1792 Unzen Mayuyama Debris Avalanches, in Abstract, 17th International Sedimentological Congress, edited by K. Hoyanagi, O. Takano, and K. Kano, p. O–152, Fukuoka., 2006.

Tibaldi, A., Corazzato, C., Kozhurin, A., Lagmay, A. F. M., Pasquarè, F. A., Ponomareva, V. V., Rust, D., Tormey, D. and Vezzoli, L.: Influence of substrate tectonic heritage on the evolution of composite volcanoes: Predicting sites of flank eruption, lateral collapse, and erosion, Glob. Planet. Change, 61(3–4), 151–174, doi:10.1016/j.gloplacha.2007.08.014, 2008.

Tibaldi, A. and Vezzoli, L.: A new type of volcano flank failure: The resurgent caldera sector collapse, Ischia, Italy, Geophys. Res. Lett., 31(14), 2–5, doi:10.1029/2004GL020419, 2004.

Ui, T.: Origin of so-called "mud-flow deposit" at northwestern slope of Gassan Volcano (in Japanese), Bull. Volcanol. Soc. Japan Second Ser., 20(2), 110, 1975.

Ui, T.: Volcanic dry avalanche deposits — Identification and comparison with nonvolcanic debris stream deposits, J. Volcanol. Geotherm. Res., 18(1–4), 135–150, doi:10.1016/0377-0273(83)90006-9, 1983.

Ui, T., Takarada, S. and Yoshimoto, M.: Debris avalanches, in Encyclopedia of Volcanoes, edited by H. Sigurdsson, B. F. Houghton, S. R. McNutt, H. Rymer, and J. Stix, pp. 617–626, Academic Press, San Diego., 2000.

Ui, T., Yamamoto, H. and Suzuki-Kamata, K.: Characterization of debris avalanche deposits in Japan, J. Volcanol. Geotherm. Res., 29(1–4), 231–243, doi:10.1016/0377-0273(86)90046-6, 1986.

Vallance, J. W. and Scott, K. M.: The Osceola Mudflow from Mount Rainier: Sedimentology and hazard implications of a huge clay-rich debris flow, Bull. Geol. Soc. Am., 109(2), 143–163, doi:10.1130/0016-7606(1997)109<0143:TOMFMR>2.3.CO;2, 1997.

Vallance, J. W., Siebert, L., Rose, W. I., Girón, J. R. and Banks, N. G.: Edifice collapse and related hazards in Guatemala, J. Volcanol. Geotherm. Res., 66(1–4), 337–355, doi:10.1016/0377-0273(94)00076-S, 1995.

Vidal, N. and Merle, O.: Reactivation of basement faults beneath volcanoes: A new model of flank collapse, J. Volcanol. Geotherm. Res., 99(1–4), 9–26, doi:10.1016/S0377-0273(99)00194-8, 2000.

Voight, B., Janda, R. J., Glicken, H. and Douglass, P. M.: Nature and mechanics of the Mount St Helens rockslide-avalanche of 18 May 1980, Géotechnique, 33(3), 243–273, doi:10.1680/geot.1983.33.3.243, 1983.

Westoby, M. J., Brasington, J., Glasser, N. F., Hambrey, M. J. and Reynolds, J. M.: "Structure-from-Motion" photogrammetry: A low-cost, effective tool for geoscience applications, Geomorphology, 179, 300–314, doi:10.1016/j.geomorph.2012.08.021, 2012.

Wooller, L., van Wyk de Vries, B., Cecchi, E. and Rymer, H.: Analogue models of the effect of long-term basement fault
5   movement on volcanic edifices, Bull. Volcanol., 71(10), 1111–1131, doi:10.1007/s00445-009-0289-3, 2009.

Yokoyama, S. and Nakagaki, Y.: Directional relation between large-scale slope failures of volcanic edifices and regional stress field (in Japanese with English abstract), J. Japan Landslide Soc., 40(1), 39–45, 2003.

Yonechi, F. and Chiba, N.: Volume of slope failure by Mt. Bandai eruption in 1888 and burial of Ura-Bandai area (in Japanese), Trans. Japanese Geomorphol. Union, 10, 72, 1989.

10   Yonechi, F., Chiba, N., Ozawa, A. and Ishimaru, S.: Large scale slope failure caused by Mt. Bandai's eruption in 1888 (in Japanese), in Abstracts of the 27th Annual Meeting of the Japan Landslide Society, pp. 20–21., 1988.

Yoshida, H.: Evaluation of sector-collapse volume of Bandai Volcano in 1888, Japan, in terms of size-distance distribution pattern of debris avalanche hummocks (in Japanese with English abstract), Trans. - Japanese Geomorphol. Union, 33(1), 45–60, 2012.

15   Yoshida, H.: Decrease of size of hummocks with downstream distance in the rockslide-debris avalanche deposit at Iriga volcano, Philippines: similarities with Japanese avalanches, Landslides, 10(5), 665–672, doi:10.1007/s10346-013-0414-4, 2013.

Yoshida, H.: Hummock alignment in Japanese volcanic debris avalanches controlled by pre-avalanche slope of depositional area, Geomorphology, 223, 67–80, doi:10.1016/j.geomorph.2014.06.024, 2014.

20   Yoshida, H. and Sugai, T.: Morphological characteristics of hummocks originating from the 24ka sector collapse event of Asama Volcano, Central Japan (in Japanese with English abstract), J. Geogr. (Chigaku Zasshi), 115(5), 638–646, doi:10.5026/jgeography.115.5_638, 2006.

Yoshida, H. and Sugai, T.: Magnitude of the sediment transport event due to the Late Pleistocene sector collapse of Asama volcano, central Japan, Geomorphology, 86(1–2), 61–72, doi:10.1016/j.geomorph.2006.08.006, 2007.

25   Yoshida, H. and Sugai, T.: Quantitative Examination of Hummock Alignment in Debris Avalanche Deposits: Zenkoji Debris Avalanche, Usu Volcano, Japan, Geogr. Rev. Japan Ser. B, 83(1), 64–72, doi:10.4157/geogrevjapanb.83.64, 2010.

Yoshida, H., Sugai, T. and Ohmori, H.: Size–distance relationships for hummocks on volcanic rockslide-debris avalanche deposits in Japan, Geomorphology, 136(1), 76–87, doi:10.1016/j.geomorph.2011.04.044, 2012.

Zernack, A. V., Procter, J. N. and Cronin, S. J.: Sedimentary signatures of cyclic growth and destruction of stratovolcanoes:
30   A case study from Mt. Taranaki, New Zealand, Sediment. Geol., 220(3), 288–305, doi:10.1016/j.sedgeo.2009.04.024, 2009.